Original Investigation

Ventricular Geometry From Non-contrast Non-ECG-gated CT Scans: An Imaging Marker of Cardiopulmonary Disease in Smokers

Farbod N. Rahaghi[1], Gonzalo Vegas-Sanchez-Ferrero[1], Jasleen K. Minhas, Carolyn E. Come, Isaac De La Bruere, James M. Wells, Germán González, Surya P. Bhatt, Brett E. Fenster, Alejandro A. Diaz, Puja Kohli, James C. Ross, David A. Lynch, Mark T. Dransfield, Russel P. Bowler, Maria J. Ledesma-Carbayo, Raúl San José Estépar[1], George R. Washko[1], the COPDGene Investigators

Rationale and Objectives: Imaging-based assessment of cardiovascular structure and function provides clinically relevant information in smokers. Non-cardiac-gated thoracic computed tomographic (CT) scanning is increasingly leveraged for clinical care and lung cancer screening. We sought to determine if more comprehensive measures of ventricular geometry could be obtained from CT using an atlas-based surface model of the heart.

Materials and Methods: Subcohorts of 24 subjects with cardiac magnetic resonance imaging (MRI) and 262 subjects with echocardiography were identified from COPDGene, a longitudinal observational study of smokers. A surface model of the heart was manually initialized, and then automatically optimized to fit the epicardium for each CT. Estimates of right and left ventricular (RV and LV) volume and free-wall curvature were then calculated and compared to structural and functional metrics obtained from MRI and echocardiograms.

Results: CT measures of RV dimension and curvature correlated with similar measures obtained using MRI. RV and LV volume obtained from CT inversely correlated with echocardiogram-based estimates of RV systolic pressure using tricuspid regurgitation jet velocity and LV ejection fraction respectively. Patients with evidence of RV or LV dysfunction on echocardiogram had larger RV and LV dimensions on CT. Logistic regression models based on demographics and ventricular measures from CT had an area under the curve of >0.7 for the prediction of elevated right ventricular systolic pressure and ventricular failure.

Conclusions: These data suggest that non-cardiac-gated, non-contrast-enhanced thoracic CT scanning may provide insight into cardiac structure and function in smokers.

Key Words: Non-ECG-gated; non-contrast; computed tomography; ventricular volume; ventricular geometry; heart; cardiac; smokers; COPD; COPDGene; congestive heart failure; echocardiography; pulmonary hypertension; right heart failure; left heart failure

Acad Radiol 2017; 24:594–602

From the Pulmonary and Critical Care Division of Department of Medicine, Brigham and Women's Hospital, 75 Francis Street, PBB—CA 3, Boston, MA 02115 (F.N.R., J.K.M., C.E.C., I.D.L.B., A.A.D., G.R.W.); Department of Radiology, Harvard School of Medicine, Boston, MA (G.V.S.-F., G.G., J.C.R., R.S.J.E.); Biomedical Image Technologies, Universidad Politécnica de Madrid & CIBER-BBN, Madrid, Spain (G.V.S.-F., M.J.L.-C.); Division of Pulmonary, Allergy and Critical Care Medicine, University of Alabama at Birmingham (J.M.W., S.P.B., M.T.D.); Division Cardiology, Department of Medicine, National Jewish Health (B.E.F.); Pulmonary and Critical Care Division of Department of Medicine, Massachusetts General Hospital (P.K.); Department of Radiology, National Jewish Health (D.A.L.); Division of Pulmonary, Critical Care and Sleep Medicine, Department of Medicine, National Jewish Health, Denver, Colorado (R.P.B.).

Received September 24, 2016; revised December 1, 2016; accepted December 2, 2016. Conception and design: GVSF, RSJE, FNR, GRW,CEC, DEL, RPB, PK; algorithmic development: GVSF, GGS, JCR, MJLC, RSJE; data collection and analysis: FNR, GVSF, JKM, IDLB, JMW, SPB, BEF, DEL, MTD, RPB; statistical analysis: FNR, CEC, AAD, GRW; manuscript preparation: FNR, GVSF, JKM, CEC, AAD, RSJE, GRW. Authors in this study were supported by NHLBI grants 5T32HL007633 (FNR), 1R01HL116931 and 5R01HL116473 (RSJE and GRW), and K08 HL123940 (JMW). [1]Equal contributors on this manuscript.
Address correspondence to: F.N.R. e-mail: frahaghi@partners.org

http://dx.doi.org/10.1016/j.acra.2016.12.007

INTRODUCTION

Cardiovascular disease is a major cause of morbidity in smokers, and as much as 50% of the estimated 24 million patients in the United States with chronic obstructive pulmonary disease (COPD) die of cardiovascular causes (1,2). Although echocardiography and cardiac magnetic resonance imaging (MRI) are often used to study cardiac structure and function in COPD (3), these are not routinely deployed in all smokers. Computed tomographic (CT) imaging of the chest is broadly used in clinical care and is increasingly used for lung cancer screening in high-risk smokers (4). Assessment of cardiac structure on those CT scans may help identify patients with COPD at greater risk of developing cardiac dysfunction. Rapid, noninvasive assessments of cardiac morphology and a better understanding of the functional interdependence of heart and lung may improve healthcare outcomes through early detection and initiation of treatment.

CT has been used to quantify coronary and thoracic aortic calcification (5), study the size of the pulmonary artery and aorta (2,6–8), and describe the relationship between pulmonary vascular and parenchymal disease progression (9,10). The caliber of other vessels such as the pulmonary veins has been explored as an image-based metric of volume status (11).

Most screening CT scans and those obtained in large multicenter studies and trials are non-electrocardiography (ECG)-gated and do not use contrast, posing significant limitation to cardiac segmentation and quantification of volume. Although previous studies of manual measurements of right ventricular-to-left ventricular (RV-to-LV) ratio have shown that ECG gating is not strictly required for the specific markers of RV dilation in pulmonary embolus, these studies still used contrast (12). Non-gated CT scans lead to cardiac motion during the scan whereby the exact boundary of the heart depends on the cardiac cycle during which the image is captured. Lack of contrast prevents simple segmentation of the ventricular septum.

Previously, we developed a method to generate a surface model of the heart from ultrasound images (13,14). We sought to adapt this methodology to non-ECG-gated and non-contrast thoracic CT scans and then explore the utility of the resulting data. We hypothesized that a model fit to the surface of the heart of non-cardiac-gated volumetric CT data could provide assessments of ventricular size, shape, and function. To test this hypothesis, we identified a subset of subjects enrolled in the Genetic Epidemiology of COPD (COPDGene) Study who underwent additional cardiac MRI or echocardiographic assessments of the heart. Whereas for the purpose of this study, the location of the heart was manually determined before deployment of the cardiac fitting algorithm, fully automated algorithms may be developed that would then permit automated objective quantification of cardiac geometry from non-contrast non-ECG-gated CT scans for further research and population screening purposes.

METHODS

COPDGene Study

The COPDGene Study has been described in detail previously (15). Briefly, it is a National Heart, Lung, and Blood Institute-funded investigation of the epidemiologic and genetic determinants of COPD in more than 10,000 current and former smokers. Subjects with active lung diseases other than COPD and asthma were excluded from participation. Each subject underwent detailed characterization including spirometric assessments of lung function. Additional data collected included self-reported physician-diagnosed medical history. Volumetric CT scans of the chest were acquired at full inspiration following the standardized COPDGene Study imaging protocol with 120 kVp, tube current of 200 mAs, and 0.5 seconds rotation time. The COPDGene study was approved by the institutional review board at each participating clinical center, and all subjects provided written informed consent.

Cardiac MRI Cohort

As part of the COPDGene Study, 24 subjects free of a documented history of pulmonary vascular or cardiac disease additionally underwent cardiac MRI (16). This cohort was used to validate the CT measurements of ventricular geometry against related measures made with MRI. Because this was a follow-up study that was not part of the initial COPDGene recruitment, the MRI images were obtained about 3 years after the CT scan was obtained. Images were obtained using a 1.5 T scanner (Signa CV/i, GE Healthcare, Milwaukee, WI). A phased array cardiac coil, prospective electrocardiographic triggering, and retrospective gating were used. Typical imaging parameters were field of view of 36–44 cm, flip angle of 35–45 degrees, matrix size of 256 in the frequency domain and 128–256 in the phase domain, relaxation time of 3.7–4.1 ms, and echocardiogram time of 1.5–1.7 ms. The end-diastolic (ED) horizontal long-axis image provided the reference from which a stack of contiguous short-axis slices of 8-mm thickness and 0-mm gap were obtained.

Echocardiography Cohort

A total of 262 patients from a single center with clinically acquired echocardiograms performed at the time of enrollment in the COPDGene Study were retrospectively identified. These subjects underwent echocardiographic assessment in addition to the standard evaluation performed at study enrollment. On average, these echocardiograms were obtained within 73 days of the CT scan. Overall RV function, estimated RV systolic pressure (RVSP), estimated LV ejection fraction (LVEF), or comments about whether the LVEF was greater than or less than 55% were documented in subsets of the echocardiogram reports. This cohort was used to study the associations between ventricular geometry acquired from CT

scan and both geometrical and functional correlates with echocardiography.

Cardiac Modeling

A detailed overview of the methodology is provided in the supplement. Briefly, we used a statistical model of the human heart that uses 50 modes of variation (non-affine deformations of cardiac structure) to describe anatomical variability (17). This model was developed from the anatomical segmentations of three-dimensional + time data sets of 138 subjects including patients without disease as well as those with a broad range of pathologic conditions to facilitate generalization of the model.

The supervised segmentation process begins with a manual initialization of the average shape model within the region of interest (performed by a trained operator) followed by an automated iteration of the deformation to optimize surface identification of the heart in the CT scan. The surface fitting is assisted by a "probabilistic driven initialization" to determine the boundary between pericardial fat and myocardium. This mode selected vertices in the normal direction of the manually initialized surface and examined the distribution of the attenuation values along those vertices in a window from −200 to 200 HU.

Based on the assumption that there are two tissues present in a single pathway (pericardial fat and then myocardium as one travels the path toward the centroid of the heart), a mixture of two components of non-central gamma distributions was fitted in the attenuation window (18,19). The lower distribution in this window represented the pericardial fat, whereas the higher attenuation distribution characterized the blood or muscle (Fig S2). Voxels are then designated as belonging to either the fat or the muscle and can be labeled as demonstrated in Figure S3.

The metrics of cardiovascular morphology extracted included the free-wall curvatures as well as estimates of the epicardial volume (wall + chamber). Endocardial volume (chamber size) for both the right and the left ventricles was estimated based on atlas models of the heart that were fitted to the epicardial surface model. Herein, these are referred to as the RV_EPI volume$_{CT}$, RV_ENDO volume$_{CT}$, LV_EPI volume$_{CT}$, and LV_ENDO volume$_{CT}$, respectively. All other measures of ventricular axes length and surface area were obtained from the epicardial surface fitting model. Sphericity was defined as:

$$Sphericity = \pi^{\frac{1}{3}} \frac{(6V)^{\frac{2}{3}}}{S}$$

where V is the volume and S is the surface area of the ventricle. The free wall was defined as the surface segments not in contact with the septum. The curvature estimate was defined as

$$\text{Curvature} = \sqrt{\frac{\left(\kappa_1^{\,2} + \kappa_2^{\,2}\right)}{2}}$$

where κ_1 is the minimum and κ_2 is the maximum curvature of the surface (20).

Statistical Analysis

Data are presented as means and standard deviations or medians and interquartile ranges where appropriate. Intra-subject stability of measures was assessed with Pearson correlation coefficients. Concordance coefficients were used to assess intra- and interoperator agreement (21). Associations between CT-derived measures of cardiac morphology and MRI- and echocardiogram-based measures of cardiac structure and function were expressed using nonparametric (Spearman) correlation coefficients. Group-to-group comparisons were evaluated using the Wilcoxon rank sum test. Logistic regression models (22) for outcomes of interest were created using a stepwise forward selection method using the measures of ventricular volume, as well as age at enrollment, gender, height, and body mass index. From these candidate variables, those with statistically significant P values using the Wald test were retained in the model. Interaction terms were included in subsequent models if they reached statistical significance or if they exhibited a P value of less than .1 and improved model performance. Logistic regression models and receiver operating characteristic curve generation were performed using Stata 14 (StataCorp, College Station, TX). All other statistical analyses were performed using SAS 9.3 (SAS Institute, Cary, NC). P values less than .05 were considered statistically significant.

RESULTS

Reproducibility of CT-based Measures of Ventricular Geometry

Data from 11 subjects who had violated study protocol by enrolling at more than one center, and thus had received CT scans at both visits, were used to assess the intra-subject reproducibility. CT-based measurements of all 11 subjects in the dual enrollment group (demographic information shown in Table 1, column A) was performed by a single operator. The second CT scan in the dual enrollment cohort occurred at a median interval of 201 days from the first scan. There was a strong correlation between the first and the second baseline measures of RV and LV volume ($R = 0.86$, $P < .001$; $R = 0.87$, $P < .001$ respectively).

The MRI cohort was used to explore the intra- and interoperator reproducibility in fitting the heart surface model to the CT scan. The demographics for the MRI cohort is shown in Table 1, column B. The mean age for this cohort was 59 ± 9 years, with a mean forced expiratory volume in 1 second of 52 ± 16% of predicted. Intraoperator agreement on assessments of RV and LV volume was excellent, with concordance coefficients of 0.92 for RV volume and 0.98 for LV volume (Table S1). Inter-concordance coefficients are

TABLE 1. Demographics of Two Cohorts Used in This Study, Both Subsets of the COPDGene Study

	(A)	(B)	(C)
	Dual Enrollment	MRI Cohort	ECHO Cohort
Variable	(*N* = 11)	(*N* = 24)	(*N* = 262)
Demographics			
Age (y)	52 ± 8	59 ± 9	65 ± 9
White race	10 (91%)	14 (58%)	250 (95%)
Male sex	11 (100%)	16 (67%)	126 (48%)
BMI	29 ± 9	29 ± 8	28 ± 7
BSA (m^2)	2.06 ± 0.25	1.99 ± 0.22	1.93 ± .28
6-minute walk distance (ft)	1105 ± 552	1069 ± 209	1173 ± 365
Lung function			
FEV_1 % predicted	70 ± 22	57 ± 27	47 ± 23
FEV_1-to-FVC ratio	0.68 ± 0.17	0.52 ± 0.16	0.46 ± 0.17
TLCpp	76 ± 20	102 ± 14	106 ± 19
(Race adjusted, L)			(*N* = 257)
MRI			
LVEF (%)		64 ± 8	
RVEF (%)		58 ± 10	
RVESVI		24 ± 9	
RVMI		13 ± 4	
ECHO			
RV minor axis			3.24 ± 0.54 (*N* = 238)
RVSP			36.0 ± 13.22
LVEF (%)			64.1 ± 7.7

BMI, body mass index; BSA, estimated body surface area; COPDGene, Genetic Epidemiology of COPD; FEV_1, forced expiratory volume in 1 second; FVC, forced vital capacity; LVEF, left ventricular ejection fraction; MRI, magnetic resonance imaging; RVEF, right ventricular ejection fraction; RVESVI, right ventricular end systolic volume index; RVMI, right ventricular mass index; TLCpp, total lung capacity, percent predicted.
Data were presented as *n* (%) and mean (±standard deviation).

TABLE 2. Correlation Coefficient (*R*) Between CT-derived Cardiac Volume Measurements and Cardiac MRI-based Volume and Mass Estimates in 24 Subjects

	Cardiac MRI-derived Metrics	
CT-derived Metrics	$RV\ ED\ Volume_{MR}$	$RV\ ED\ Mass_{MR}$
$RV\_EPI\ Volume_{CT}$	0.65 (.0006)	0.60 (.002)
$RV\_ENDO\ Volume_{CT}$	0.61 (.001)	0.57 (.004)
	$LV\ ED\ volume_{MR}$	$LV\ ED\ mass_{MR}$
$LV\_EPI\ volume_{CT}$	0.61 (.001)	0.56 (.004)
$LV\_ENDO\ volume_{CT}$	0.60 (.002)	0.51 (.01)
	$LV\ ED\ length_{MR}$	
$LV\ Long\ Axis_{CT}$	0.49 (.02)	
	$LV\ mid\ ED\ curvature_{MR}$	
LV Free Wall $curvature_{CT}$	0.70 (.0001)	
	$LV\ ED\ radius\ ratio_{MR}$	
$LV\ sphericity_{CT}$	0.51 (.01)	
	$RV/LV\ ED\ volume\ ratio_{MR}$	
$RV/LV\ volume\ ratio_{CT}$	0.46 (.02)	

CT, computed tomographic; ED, end diastolic; LV, left ventricular; MID, middle of ventricle; MRI, magnetic resonance imaging; RV, right ventricular.
Spearman correlation coefficients, with accompanying *P* values.

shown in Table S2, with concordance coefficients ranging from 0.91 to 0.97.

Validation of CT-based Ventricular Geometry as Compared to MRI Measures

The associations of CT and MRI assessments of ventricular dimensions were explored using data from MRI cohort and is presented in Table 2. The CT-based estimates of RV volume ($RV\_EPI\ volume_{CT}$ and $RV\_ENDO\ volume_{CT}$) were significantly associated with both the ED RV volume ($RV\ ED\ volume_{MR}$) and the mass ($RV\ ED\ mass_{MR}$) obtained from MRI. There were similarly significant associations between CT and MRI LV measures. CT-based estimates of the long-axis dimension of the LV ($LV\ Long\ Axis_{CT}$) were related to this same measure ($LV\ ED\ length_{MR}$) obtained from MR as were measures of the free-wall curvature of the ventricle (LV Free Wall $curvature_{CT}$ and $LV\ mid\ ED\ curvature_{MR}$). The sphericity of the LV on CT scan ($LV\ sphericity_{CT}$) was also significantly related to the long- to short-axis radius ratio of the LV obtained from MRI ($LV\ ED\ radius\ ratio_{MR}$). Finally, the CT-derived ratio of RV-to-LV volume ($RV\text{-}to\text{-}LV\ volume\ ratio_{CT}$) was significantly associated with the ratio of those same measures obtained from MRI ($RV/LV\ ED\ volume\ ratio_{MR}$).

Association Between CT-based Ventricular Geometry and Echocardiographic-based Ventricular Structure and Function

Examples of chamber models reconstructed for three subjects with echocardiograms are shown in Figure 1. The mean age for the echocardiogram cohort was 64.7 ± 9 years with a mean forced expiratory volume in 1 second of 47 ± 23% predicted (additional demographic information in Table 1, column C). The $RV\ Long\ Axis_{CT}$ and the $RV\ short\ Axis_{CT}$ were significantly associated with $RV\ Minor\ axis_{ECHO}$ obtained from echocardiography. The RV_EPI and $RV\_ENDO\ volume_{CT}$ and $RV\ surface\ area_{CT}$ were also related to echocardiogram-derived axis measurements. One hundred and ninety-four of the 262 echocardiograms reported an estimated RVSP. This RVSP was directly related to CT measures of RV size ($RV\_EPI\ volume_{CT}$, $RV\_ENDO\ volume_{CT}$, $RV\ Long\ Axis_{CT}$, $RV\ Short\ Axis_{CT}$, and $RV\ surface\ area_{CT}$). In addition, 130 of the echocardiogram reports were noted to have descriptions of RV function as being normal ($n = 120$) or decreased ($n = 10$). There were statistically significant differences in the CT-based measures of RV size in those with decreased RV function versus those with preserved function (Table 3).

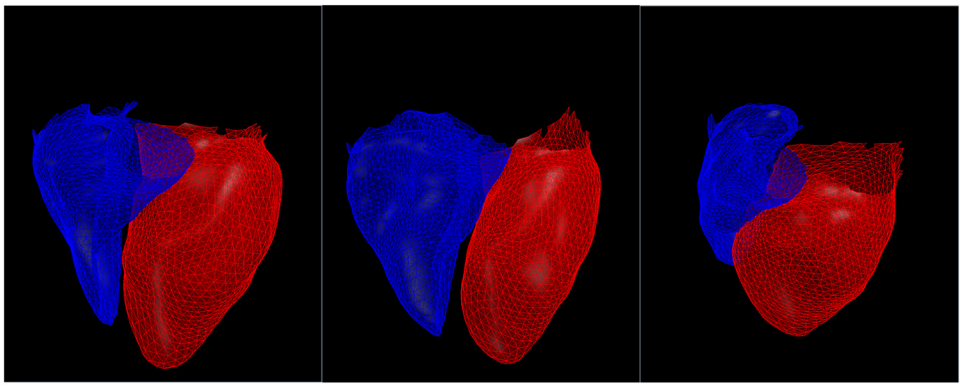

Figure 1. The right ventricle (*blue*) and left ventricle (*red*) in three subjects with a cardiac model fitted to the surface of the heart using volumetric non-contrast computed tomographic scan. A subject with Gold 0 disease and with a right ventricular-to-left ventricular (RV-to-LV) ratio of 0.5, RV systolic pressure (RVSP) of 20 and no evidence of ventricular dysfunction **(a)**, subject with Gold 3 disease and RV/LV ratio of 0.8, RV dilation, elevated RVSP of 47 **(b)**, and subject with Gold 2 disease with LV dilation and ejection fraction of 35% **(c)**.

TABLE 3. Correlation of CT-derived Right Ventricular Geometry With Echocardiogram-derived Geometric and Functional Measures (First Three Columns) and the Difference in Those Metrics Between Patients Characterized as Having Abnormal Versus Patients Having Normal RV Function

	Echocardiogram-derived Measures				
CT-derived Measures of Right Ventricle	RV Minor $Axis_{ECHO}$ ($N = 238$)	RVSP ($N = 194$)	Decreased RV Function ($N = 10$)	Normal RV Function ($N = 120$)	*P*
RV Long $Axis_{CT}$	$R = 0.36$, $P < .0001$	$R = 0.28$, $P < .0001$	7.3[6.1–7.5]	6.9[6.4–7.3]	.44
RV short $Axis_{CT}$	$R = 0.44$, $P < .0001$	$R = 0.27$, $P = .0002$	4.3[4.0–4.7]	4.0[3.6–4.3]	.03
RV_EPI $volume_{CT}$	$R = 0.46$, $P < .0001$	$R = 0.3$, $P < .0001$	106[87–117]	85[66–103]	.04
RV_ENDO $volume_{CT}$	$R = 0.45$ $P < .0001$	$R = 0.28$ $P = .0001$	67[54–79]	57[42–67]	.06
RV surface $area_{CT}$	$R = 0.49$, $P < .0001$	$R = 0.24$, $P = .0006$	169[142–194]	148[130–169]	.05

CT, computed tomographic; RA, right atrium; RV, right ventricle; RVSP, estimated right ventricular systolic pressure by echocardiogram. Values shown are Spearman correlation coefficients (*R*) and *P* values associated with Spearman correlation. Values shown for subgroups with decreased and normal RV function are shown as median [interquartile range].

A subset of the echocardiogram reports also provided an additional qualitative description of LV function ($n = 180$ where the LV function was categorized as "normal" or "reduced"), whereas some had quantitative estimates of the LVEF ($n = 98$ subjects). There were statistically significant differences in the CT estimates of LV size and morphology between subjects with reduced LV function ($N = 18$) and those with normal LV function ($N = 162$) (Table 4). Subjects with a reduced EF had larger LV size with lesser free-wall curvature on CT scan. In the subjects with quantitative measurement of LVEF, a larger LV size and reduced free-wall curvature were also predictive of reduced LVEF.

Logistic regression models were constructed for the following variables: elevated RVSP (RVSP > 40 mm Hg), reduced RV function, and reduced LVEF (Table 5). RV volume was a statistically significant predictor of both RVSP and RV failure, with gender and age being independent predictors and effect modifiers of this association. The final model for RVSP, which included RV volume, age, gender, and the interaction terms, had an area under the curve (AUC) of 0.77. The final model for RV failure included age and gender and had an AUC of 0.76. LV volume (LV_EPI $volume_{CT}$) was predictive of decreased LVEF, and with the addition of body mass index, the final model had an AUC of 0.71.

TABLE 4. Correlation of CT-derived Left Ventricular Geometry With Echocardiogram-derived Functional Measures (First Three Columns) and the Difference in Those Metrics Between Patients Characterized as Having Abnormal Versus Patients Having Normal Left Ventricular Ejection Fraction

	ECHO-derived Measures			
CT Measures of Left Ventricle	LVEF ($N = 98$)	Reduced EF ($N = 18$)	Normal EF ($N = 162$)	*P* Value
LV Long $Axis_{CT}$	$R = -0.20$, $P = .05$	8.54[7.69–9.21]	8.05[7.42–8.62]	.08
LV_EPI $volume_{CT}$	$R = -0.22$, $P = .03$	207.1[167.5–240.1]	173.1[143.8–199.2]	.01
LV_ENDO $volume_{CT}$	$R = -0.23$, $P = .03$	118.0[89.0–141.1]	97.1[78.4–111.6]	.02
LV surface $area_{CT}$	$R = -0.21$, $P = .03$	202.7[164.1–223.7]	176.6[153.1–197.0]	.03
LV volume/surface $Area_{CT}$	$R = -0.18$, $P = .08$	1.03[0.98–1.07]	0.97[0.92–1.02]	.009
LV Free-Wall $Curvature_{CT}$	$R = 0.20$, $P = .04$	0.018[0.0169–0.0195]	0.0192[0.18-0.0205]	.03

EF, ejection fraction; LV, left ventricle.

Values shown are correlation coefficients (*R*) and *P* values associated with Spearman correlation. Values shown for subgroups with decreased and normal ejection fraction are shown as median [interquartile range].

TABLE 5. Logistic Regression Model Performance Based on AUC (Area Under the Curve) for Models Predicting RVSP >40, Reduced RV Function, Reduced LV Ejection Fraction, and History of CHF

	RVSP >40	RVF	Reduced LVEF	
	$N = 194$	$N = 130$	$N = 180$	
	(64/194)	(10/130)	(18/180)	
Model Variables	AUC	AUC	Model Variables	AUC
RVV	0.67	0.70	LVV	0.68
RVV+Age+Gender	0.75	0.75	LVV+BMI	0.71
RVV+Age+Gender +RVV*Gender	0.77			

LV, left ventricle; LVEF, left ventricular ejection fraction; LVV, left ventricle volume; RV, right ventricle; RVF, evidence of RV failure on echocardiogram; RVSP, estimated right ventricular systolic pressures by echocardiogram; RVV, right ventricle volume.

DISCUSSION

CT characterization of thoracic disease in smokers is increasingly leveraged for clinical, epidemiologic, and genetic investigation. Whereas previous investigations have demonstrated the utility of CT-based assessments of the vascular tree and atherosclerosis in smokers, little literature exists on directly modeling the heart from non-ECG-gated, noncontrast CT data. Herein we report the development and application of a model of cardiac structure based on a surface fitting algorithm applied to non-cardiac-gated, non-contrast-enhanced images. From this initial fit of the epicardial surface, we made inferences about the right and the left epicardial (wall and chamber) as well as endocardial (chamber) ventricular size and shape. We found that CT-based measures of RV and LV shape and size were significantly associated with MRI and echocardiogram-based assessments of these same chambers. We further found that such CT-based morphology had discriminatory power in detecting abnormal ventricular function detected by echocardiography.

MRI is considered a gold standard for the noninvasive assessment of the cardiac structure. It can provide detailed assessments of ventricular morphology and function without decrements in image quality that are observed using echocardiography in hyperinflated patients with COPD. Using data from 24 subjects who underwent CT and MRI, we found highly statistically significant associations between CT- and MR-based measures of ventricular size and morphology. Up to 50% of the variance in the MRI-based measures of ventricular structure was explained by the CT data. These associations were strongest with CT-based measures of LV free-wall curvature and tended to weaken with measures of volume. The latter is not surprising because the CT-based model relies on statistical inference of septal location and morphology. Because the cardiac MRI studies were obtained 3 years after the CT data, changes in the cardiovascular state of the subjects in the interim could also introduce a difference between the two measurements.

There were also significant associations between our CT measures of ventricular morphology and similar assessments obtained from echocardiography. These correlations were of the same direction and magnitude as those observed in the MRI data. The larger sample size of echocardiogram data allowed additional exploration of CT structure and cardiac function. In these data, we again found highly plausible associations. Subjects with larger RVs on CT were more likely to have elevated pulmonary arterial pressures (estimated by RVSP) and decreased RV function. Subjects with an enlarged left ventricle and reduced curvature of the free wall on CT scan tended to have lower estimated LVEFs on echocardiogram. These findings were further corroborated in regression models adjusted for subject age and sex, where the AUCs were greater than 0.75 (Fig 2). We suspect that the reasons for this are not found in the detection of cardiac displacement on CT but rather in the relationship between

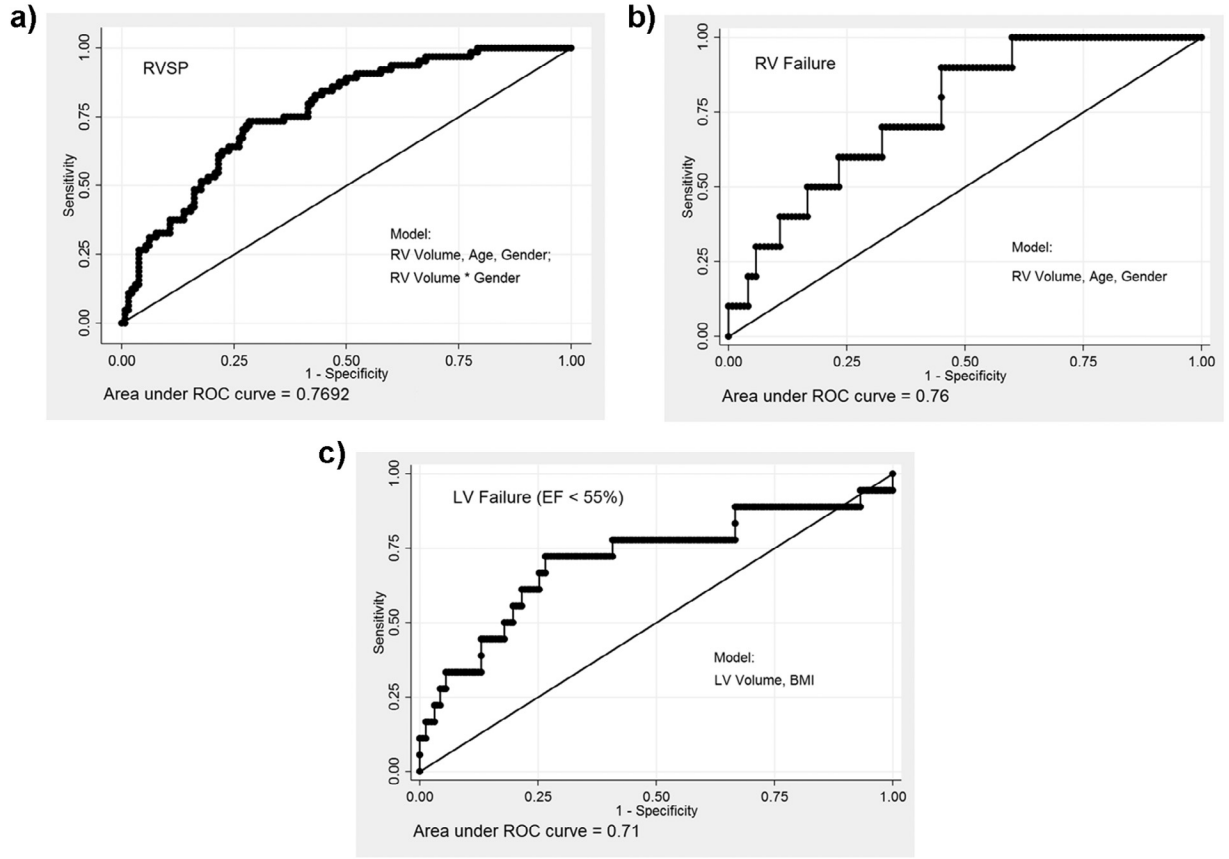

Figure 2. Model discrimination performance as measured by the area under the receiver operating characteristic curve, shown for four logistic regression models constructed using a stepwise forward selection method for markers of cardiac dysfunction in the cohort with available echocardiograms. A model of ability to predict right ventricular (RV) systolic pressure ≥40 **(a)**, RV failure as marked on the echocardiogram **(b)**, and left ventricular failure defined by ejection fraction <55% **(c)**.

chamber structure and function. Deviations in structure likely connote deviations in function where, for example, an enlarged left ventricle is less likely to exhibit a normal EF.

There are several limitations to this work that must be acknowledged. The first is the nature of the data obtained from the CT-based surface fitting model. Because the cardiac structures below the epicardial surface are indiscernible on non-contrast-enhanced, non-cardiac-gated CT scans, metrics of RV and LV size were highly dependent on accurate estimates of the location of the inter-ventricular septum. This is likely why the strongest correlations between CT and MR tended to be those assessing surface morphology rather than volume. CT scans were obtained with an inspiratory hold, whereas measurements in cardiac MRI are often obtained during expiratory breath-holds. The type of breath-hold used in cardiac MRI and echocardiography can significantly alter diaphragm position and preload, thus altering measurements of chamber geometry. It must also be noted that the measures of curvature from the MRI were obtained from the cardiac MRI report and were not replicated using our techniques. It is highly likely that there are differences in the location and technique used to assess free-wall curvature between the CT and the MRI data. Subtle differences in such techniques may result in large differences in estimates given the eccentric surface of the ventricles. The association of CT- and MRI-based measures of ventricular morphology would likely be further improved if the same operator performed the assessments using a single technique. Another limitation to this investigation is the number of subjects and timing of the MRI data collection, which was obtained 3 years after the CT scan. Although this likely introduced a source of error in the comparison between cardiac MRI and CT scan, there is no a priori reason to suspect that this would lead to overestimating the agreement between the two modalities, whereas it is likely that it may have accounted for part of the discrepancy between the two measurements. The small sample size prevented detailed examination of CT morphology and MRI measures of cardiac function. Progression of disease and changes in volume status between the two imaging time points complicated this comparison.

In conclusion, estimates of RV and LV size and morphology can be obtained from volumetric CT data. These measures are associated with structural and functional data obtained from MRI and echocardiographic techniques. These techniques have the capability of becoming fully automated and incorporated into the clinical reporting of CT data. Significant numbers

of CT scans are obtained in patients with lung disease, dyspnea, and smokers, all of whom are at risk of cardiovascular disease, and in the appropriate clinical settings, findings of abnormal cardiac geometry on CT scan would then warrant further cardiac examination. Cohorts specifically designed for assessing the performance of these methods in screening for cardiovascular disease are necessary to validate and optimize this method and to minimize unnecessary follow-up testing while improving clinical value. Additionally, methods of automated quantification of cardiac geometry can be broadly deployed in CT-based clinical, epidemiologic, and genetic investigations of diseases affecting the chest.

REFERENCES

1. Divo M, Cote C, de Torres JP, et al. Comorbidities and risk of mortality in patients with chronic obstructive pulmonary disease. Am J Respir Crit Care Med 2012; 186:155–161.
2. Sin DD, Man SF. Chronic obstructive pulmonary disease as a risk factor for cardiovascular morbidity and mortality. Proc Am Thorac Soc 2005; 2:8–11.
3. Rahaghi FN, van Beek EJ, Washko GR. Cardiopulmonary coupling in chronic obstructive pulmonary disease: the role of imaging. J Thorac Imaging 2014; 29:80–91.
4. Eberth JM. Lung cancer screening with low-dose CT in the United States. J Am Coll Radiol 2015; 12:1395–1402.
5. Budoff MJ, Nasir K, Kinney GL, et al. Coronary artery and thoracic calcium on noncontrast thoracic CT scans: comparison of ungated and gated examinations in patients from the COPD Gene cohort. J Cardiovasc Comput Tomogr 2011; 5:113–118.
6. Wells JM, Washko GR, Han MK, et al. Pulmonary arterial enlargement and acute exacerbations of COPD. N Engl J Med 2012; 367: 913–921.
7. Ng CS, Wells AU, Padley SP. A CT sign of chronic pulmonary arterial hypertension: the ratio of main pulmonary artery to aortic diameter. J Thorac Imaging 1999; 14:270–278.
8. Kurugol S, Come CE, Diaz AA, et al. Automated quantitative 3D analysis of aorta size, morphology, and mural calcification distributions. Med Phys 2015; 42:5467–5478.
9. Matsuoka S, Washko GR, Yamashiro T, et al. Pulmonary hypertension and computed tomography measurement of small pulmonary vessels in severe emphysema. Am J Respir Crit Care Med 2010; 181:218–225.
10. Estepar RS, Kinney GL, Black-Shinn JL, et al. Computed tomographic measures of pulmonary vascular morphology in smokers and their clinical implications. Am J Respir Crit Care Med 2013; 188:231–239.
11. Smith BM, Prince MR, Hoffman EA, et al. Impaired left ventricular filling in COPD and emphysema: is it the heart or the lungs? The Multi-Ethnic Study of Atherosclerosis COPD Study. Chest 2013; 144:1143–1151.
12. Lu MT, Cai T, Ersoy H, et al. Comparison of ECG-gated versus nongated CT ventricular measurements in thirty patients with acute pulmonary embolism. Int J Cardiovasc Imaging 2009; 25:101–107.
13. Haak A, Ren B, Mulder HW, et al. Improved segmentation of multiple cavities of the heart in wide-view 3-D transesophageal echocardiograms. Ultrasound Med Biol 2015; 41:1991–2000.
14. Haak AM, Mulder HW, Ren B, et al. Segmentation of multiple heart cavities in wide-view fused 3D transesophageal echocardiograms. In: Ultrasonics symposium (IUS), 2014 IEEE international. 2014; 691–694.
15. Regan EA, Hokanson JE, Murphy JR, et al. Genetic epidemiology of COPD (COPDGene) study design. COPD 2010; 7:32–43.
16. Wells JM, Iyer AS, Rahaghi FN, et al. Pulmonary artery enlargement is associated with right ventricular dysfunction and loss of blood volume in small pulmonary vessels in chronic obstructive pulmonary disease. Circ Cardiovasc Imaging 2015; 8.
17. Hoogendoorn C, Duchateau N, Sanchez-Quintana D, et al. A high-resolution atlas and statistical model of the human heart from multislice CT. IEEE Trans Med Imaging 2013; 32:28–44.
18. Vegas-Sanchez-Ferrero G, Aja-Fernandez S, Palencia C, et al. A generalized gamma mixture model for ultrasonic tissue characterization. Comput Math Methods Med 2012; 2012:481923.
19. Vegas-Sanchez-Ferrero G, Seabra J, Rodriguez-Leor O, et al. Gamma mixture classifier for plaque detection in intravascular ultrasonic images. IEEE Trans Ultrason Ferroelectr Freq Control 2014; 61:44–61.
20. Koenderink JJ, van Doorn AJ. Surface shape and curvature scales. Image Vis Comput 1992; 10:557–564.
21. Lin LI. A concordance correlation coefficient to evaluate reproducibility. Biometrics 1989; 45:255–268.
22. Hosmer DW, Lemeshow S, Sturdivant RX, eds. Applied logistic regression. third ed. New Jersey: John Wiley & Sons, Inc., 2013.

APPENDIX. SUPPLEMENTARY DATA

Supplementary data related to this article can be found at http://dx.doi.org/10.1016/j.acra.2016.12.007.